

This document is confidential and is proprietary to the American Chemical Society and its authors. Do not copy or disclose without written permission. If you have received this item in error, notify the sender and delete all copies.

Organic covalent patterning of nanostructured graphene with selectivity at the atomic level

Journal:	<i>Nano Letters</i>
Manuscript ID	nl-2015-03928e.R1
Manuscript Type:	Communication
Date Submitted by the Author:	n/a
Complete List of Authors:	Navarro, Juan Jesús; IMDEA Nanociencia Leret, Sofia; IMDEA Nanociencia Calleja, Fabian; IMDEA Nanociencia Stradi, Daniele; Instituto Madrileño de Estudios Avanzados en Nanociencia (IMDEA Nanociencia); Universidad Autonoma de Madrid, Departamento de Quimica Modulo13 Black, Andrés; Universidad Autonoma de Madrid, Fisica de la Materia Condensada; IMDEA Nanociencia Bernardo-Gavito, Ramón; Universidad Autonoma de Madrid, Fisica de la Materia Condensada; IMDEA Nanociencia Garnica, Manuela; IMDEA Nanociencia; Universidad Autonoma de Madrid, Fisica de la Materia Condensada Granados, Daniel; IMDEA Nanociencia Vazquez de Parga, Amadeo; Universidad Autonoma de Madrid, Fisica de la Materia Condensada Pérez, Emilio; IMDEA Nanoscience, Miranda, Rodolfo; Universidad Autonoma de Madrid; IMDEA Nanociencia

SCHOLARONE™
Manuscripts

Organic covalent patterning of nanostructured graphene with selectivity at the atomic level

Juan Jesús Navarro^a, Sofía Leret^a, Fabián Calleja^a, Daniele Stradi^{a,b,†}, Andrés Black^{a,c}, Ramón Bernardo-Gavito^{a,c}, Manuela Garnica^{a,c,‡}, Daniel Granados^a, Amadeo L. Vázquez de Parga^{a,c,}, Emilio M. Pérez^{a,*}, Rodolfo Miranda^{a,c}.*

^a IMDEA Nanociencia, Calle Faraday 9, Cantoblanco 28049, Madrid, Spain

^b Departamento de Química, Módulo13, Universidad Autónoma de Madrid, Cantoblanco 28049, Madrid, Spain

^c Departamento de Física de la Materia Condensada and IFIMAC, Universidad Autónoma de Madrid, Cantoblanco 28049, Madrid, Spain.

ABSTRACT. Organic covalent functionalization of graphene with long-range periodicity is highly desirable –it is anticipated to provide control over its electronic, optical, or magnetic properties– and remarkably challenging. In this work we describe a method for the covalent modification of graphene with strict spatial periodicity at the nanometer scale. The periodic landscape is provided by a single monolayer of graphene grown on Ru(0001), that presents a moiré pattern due to the mismatch between the carbon and ruthenium hexagonal lattices. The moiré contains periodically arranged areas where the graphene-ruthenium interaction is enhanced and shows higher chemical reactivity. This phenomenon is demonstrated by the attachment of

1
2
3 cyanomethyl radicals ($\text{CH}_2\text{CN}^\bullet$) produced by homolytic breaking of acetonitrile (CH_3CN), which
4
5 is shown to present a nearly complete selectivity (>98 %) to bind covalently to graphene on
6
7 specific atomic sites. This method can be extended to other organic nitriles, paving the way for
8
9 the attachment of functional molecules.
10
11

12
13
14 KEYWORDS: nanostructured graphene, epitaxial graphene, chemical functionalization,
15
16 scanning tunneling microscopy
17
18
19
20
21
22
23
24
25
26
27
28
29
30
31
32
33
34
35
36
37
38
39
40
41
42
43
44
45
46
47
48
49
50
51
52
53
54
55
56
57
58
59
60

1
2
3 Graphene is a bidimensional network of sp^2 -hybridized carbon atoms. The planar hexagonal
4
5 arrangement of carbon in graphene, its chemical stability, and most significantly, its
6
7 extraordinary physical properties all stem from the extended conjugation provided by the
8
9 homogeneous sp^2 hybridization.¹ The chemical functionalization of graphene has been intensely
10
11 pursued in the last years.^{2,3} A significant part of the research efforts from the wet chemistry
12
13 trench have focused on the covalent attachment of molecular fragments to graphene. Addition of
14
15 malonate-type carbanions and radicals, acylations, and a wide variety of cycloadditions,
16
17 including [2+1], [2+2], [3+2], and [4+2], have all been explored, among others.⁴⁻⁷ Negative
18
19 consequences of graphene's planar geometry are its insolubility and its tendency to reaggregate
20
21 to form graphite through π - π and van der Waals interactions. Such issues can be solved using
22
23 graphene on a suitable substrate (for a recent review see Criado et al⁸). It has been demonstrated
24
25 that graphene grown or deposited on a substrate can physisorb or chemisorb molecules. Weakly
26
27 attached adsorbates can act as donors or acceptors leading to changes in carrier concentration
28
29 that allow the detection of single molecules⁹ or the formation of intermolecular bands with long
30
31 range magnetic order at low temperatures.¹⁰ Beyond the supramolecular functionalization of
32
33 epitaxial graphene, its covalent modification has been proposed as an ideal tool for adjusting the
34
35 electronic, optical or magnetic properties. The chemical oxidation of graphene in ultra-high
36
37 vacuum (UHV) conditions has also been demonstrated.^{11,12} The attachment of hydrogen to each
38
39 atomic site of the graphene lattice to create graphane was proposed,¹³ resulting in a change in the
40
41 hybridization of carbon atoms from sp^2 to sp^3 , as well as the opening a sizeable gap at the
42
43 Dirac point.¹⁴⁻¹⁶ In these experiments, all the atoms in the graphene lattice exhibit very similar
44
45 reactivity and the only way to get an atomically well-defined long range order is to saturate all
46
47 the atomic sites, creating a completely new material, e.g. graphane or graphene oxide. This lack
48
49
50
51
52
53
54
55
56
57
58
59
60

1
2
3 of selectivity is a major drawback if the objective of the covalent modification is to modulate the
4
5
6
7
8
9
10
11
12
13
14
15
16
17
18
19
20
21
22
23
24
25
26
27
28
29
30
31
32
33
34
35
36
37
38
39
40
41
42
43
44
45
46
47
48
49
50
51
52
53
54
55
56
57
58
59
60

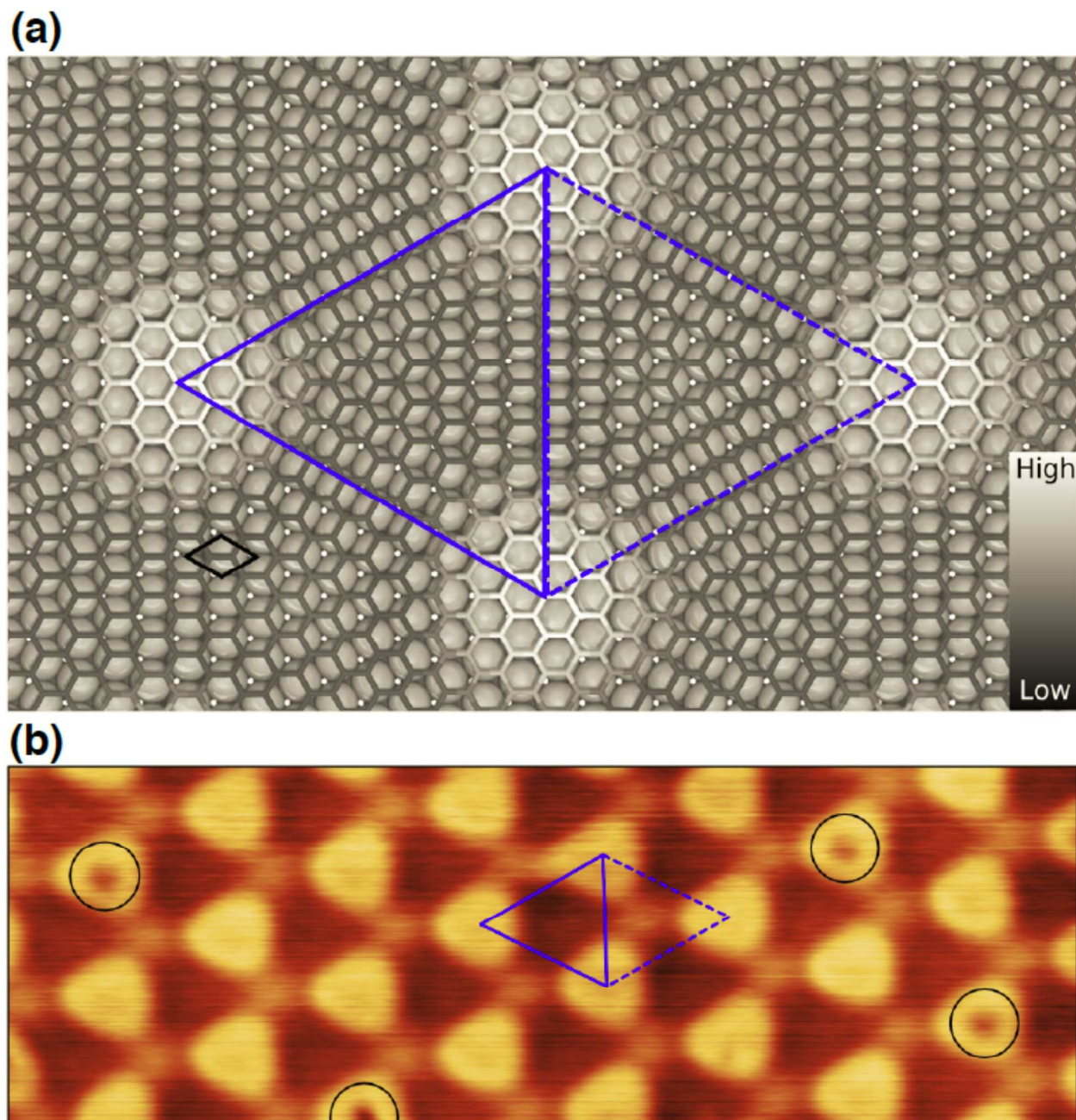
of selectivity is a major drawback if the objective of the covalent modification is to modulate the electronic properties of graphene. It has been predicted that a periodic patterning of graphene would lead to new electronic properties¹⁷ including a direct relation between the periodicity and the bandgap amplitude.^{18,19} Therefore the chemical functionalization of graphene in a periodic fashion with a periodicity in the range of 1 to 5 nm is highly desirable.

There have been several approaches for obtaining site selectivity in the chemical functionalization of graphene. One approach relies on patterning the surface using an atomic force microscope (AFM).^{20,21} The main drawback of this approach is the time needed to write the motifs and also the difficulty of scaling the process to millimetre size samples. Another approach relies on the fact that strain and curvature strongly enhance the local reactivity of the graphene,^{22,23} although so far no long range order has been achieved. Graphene grown on metallic substrates presents a moiré pattern due to the difference in lattice parameter between graphene and the substrate.²⁴ In particular, graphene grown on Ir(111) has been used to study the influence of a spatially ordered covalent functionalization in the graphene electronic structure.^{25,26} Due to the weak interaction between the graphene and the Ir(111) substrate, the moiré pattern presents several rotational domains with different periodicities.^{27,28} The weak interaction with the substrate also renders all the carbon atoms almost identical electronically and no distinct reactive sites are present in the system. To the best of our knowledge, there have been no reports of covalent functionalization of graphene with atomic-level selectivity.

Here, we describe a method for the organic covalent modification of graphene with exquisite spatial periodicity at the atomic scale. We take advantage of the fact that the growth of graphene on lattice-mismatched metallic substrates allows us to tailor the geometric and electronic properties of the graphene overlayer in a periodic fashion. In particular, we use graphene grown

1
2
3 on Ru(0001) that presents a moiré pattern with a periodicity of ≈ 3 nm. The moiré shows
4 periodically distributed areas where the charge transfer due to the interaction between graphene
5 and ruthenium is rather large and, as a consequence, these graphene areas present higher
6 chemical reactivity. This point is illustrated by demonstrating that cyanomethyl radicals
7 ($\text{CH}_2\text{CN}^\bullet$) produced by homolytic breaking of acetonitrile (CH_3CN) in UHV by electron
8 bombardment bind to graphene preferentially at specific atomic sites with a nearly complete
9 selectivity (>98%).
10
11
12
13
14
15
16
17
18
19

20
21 Growth of graphene through chemical vapour deposition (CVD) on a variety of metallic
22 substrates is one of the preferred methods for the synthesis of high-quality graphene.²⁹⁻³² This
23 method presents the additional advantage that the strength in the interaction between graphene
24 and the metallic substrate can be tuned by varying the chemical nature of the latter.³³ In this
25 respect some of us have previously reported the epitaxial growth of graphene on Ru(0001)
26 (hereafter, gr/Ru(0001)) where due to the mismatch between the hexagonal lattices of graphene
27 and Ru, the system presents a moiré pattern with a surface periodicity of 2.93 nm³⁴ (see
28 Supporting Information A for further details). Figure 1(a) shows that three different areas can be
29 distinguished inside the moiré unit cell depending on the registry between the carbon atoms and
30 the last two ruthenium atomic layers, namely: the "atop" region where all carbon atoms are
31 placed above threefold hollow sites of the Ru surface (vertex of the blue triangles in Fig. 1(a)),
32 the "HCP-Top" region where half of the carbon atoms are located on HCP threefold positions
33 and the other half on top of Ru atoms (dashed blue triangle in Fig. 1(a)) and the "FCC-Top"
34 region where half of the carbon atoms are located on FCC threefold positions and the other half
35 on top of Ru atoms (solid blue triangle in Fig. 1(a)).
36
37
38
39
40
41
42
43
44
45
46
47
48
49
50
51
52
53
54
55
56
57
58
59
60



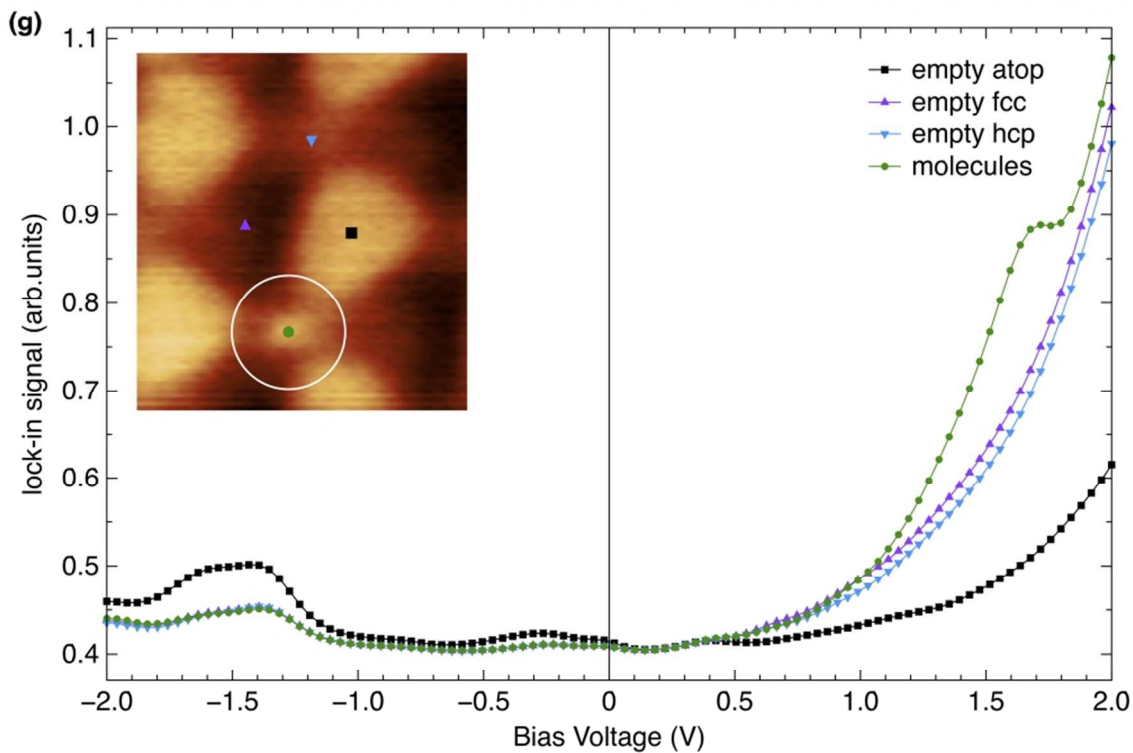
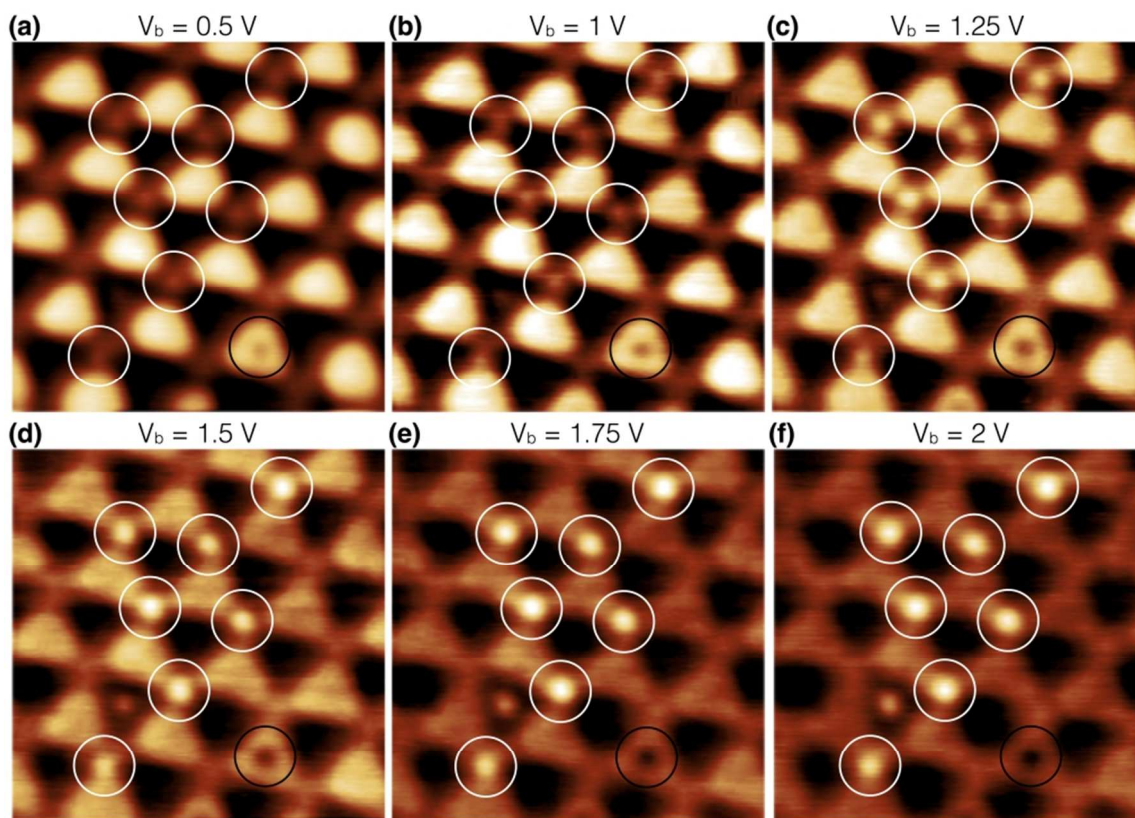
47 **Figure 1.** (a) Ball model of the gr/Ru(0001) surface, where grey circles represent the Ru atoms
48 of the first atomic layer. The graphene hexagonal lattice is shown in a black to white color scale
49 to indicate the height of the carbon atoms respect to the Ru(0001) surface. The unit cell of the
50 moiré pattern is highlighted by two blue triangles. At the vertices all carbon atoms fall on
51 threefold hollow sites of the Ru(0001) surface. At the center of the solid (dashed) triangle one
52
53
54
55
56
57
58
59
60

1
2
3 carbon sub-lattice falls on FCC-stacked (HCP-stacked) threefold hollow sites and the other one
4
5 on top positions. These two regions are named “FCC-Top” and “HCP-Top” respectively. (b)
6
7 STM image acquired on pristine gr/Ru(0001) ($24 \times 7 \text{ nm}^2$; $V_b = +1.5 \text{ V}$, $I_t = 30 \text{ pA}$). The moiré
8
9 pattern arising from the lattice mismatch is highlighted in blue. The HCP-Top area is marked
10
11 with the dashed triangle and the FCC-Top area is marked the solid triangle. Four point defects on
12
13 the atop areas are indicated by black circles.
14
15

16
17
18 Figure 1(b) shows a Scanning Tunneling Microscope (STM) topographic image of the surface
19
20 measured at +1.5V bias voltage. Under these bias conditions, the moiré appears as a hexagonal
21
22 array of bumps with a small corrugation ($\sim 40 \text{ pm}$). The origin of the bumps is the change in
23
24 registry within the moiré unit cell that produces a spatial modulation in the interaction between
25
26 the C and Ru atoms, from weak van der Waals interaction in the high areas of the STM images to
27
28 strong interaction in the lower areas.^{35,36} This spatial variation of the interaction modulates all
29
30 surface electronic properties, from the surface potential³⁷ to the electronic structure around the
31
32 Fermi level,³⁴ which directly affects the chemical reactivity. The STM imaging conditions of
33
34 Figure 1b also reveal the presence of four point defects on top of the ripples (marked with black
35
36 circles), which we attribute to subsurface oxygen trapped during the graphene growth process
37
38 (see Supporting Information B for details).
39
40
41
42
43
44

45
46 Recently, Ruoff, Bielawsky and co-workers have introduced a method for the selective
47
48 functionalization of graphene on areas with high local curvature.²² Considering this, and the
49
50 seminal work by Balog et al. on the patterned hydrogenation of graphene on Ir,²⁵ we reasoned
51
52 that graphene on Ru(0001) seems an ideal playground to exploit a similar strategy for a *periodic*
53
54 chemical modification of graphene with sub-nanoscale selectivity. The metal-graphene
55
56 interaction in gr/Ru(0001) is sufficiently strong to affect the chemical reactivity of specific
57
58
59
60

1
2
3 atomic sites of the graphene overlayer, due to the presence of the moiré-related corrugation.
4
5 While attempting to reproduce the wet-chemistry reaction conditions, we serendipitously
6
7 discovered that gr/Ru(0001) can be functionalized by cyanomethyl radicals with exquisite spatial
8
9 selectivity (see Supporting Information C for details). Representative STM images are shown in
10
11 Figure 2a-f, measured at 80 K as a function of the sample bias voltage after exposure of the
12
13 sample at room temperature to 1×10^{-6} Torr of CH₃CN for 3 minutes, equivalent to 180
14
15 Langmuirs. Bright bumps related to the adsorption of acetonitrile, located exclusively at the
16
17 valleys and the HCP-top sites, are observed for voltages between +1.25 V and +2 V. The
18
19 molecular attachments show an apparent height of 26 ± 2 pm and a lateral width of 560 ± 20 pm
20
21 at +1.5 V. The shape and size of the molecular attachments are very similar to those measured
22
23 on STM images taken of acetonitrile adsorbed on Pt(111).³⁸ Figure 2(g) shows Scanning
24
25 Tunnelling Spectroscopy (STS) recorded on various positions of the moiré unit cell. The curves
26
27 measured on top of the ripples and the ones measured on the (empty) low areas of the moiré
28
29 show the well-known asymmetry between the occupied and empty density of states of
30
31 gr/Ru(0001).³⁴ The curves measured on the molecular attachments present an additional peak at
32
33 +1.6 eV identified as the Lowest Unoccupied Molecular Orbital (LUMO). The energy of the
34
35 Highest Occupied Molecular Orbital (HOMO) is below -2.0 V and, therefore, out of the
36
37 measured energy window. The images confirm that for bias voltages below +0.5 V the molecular
38
39 attachments are not visible, since tunneling is being carried out in the gap between the HOMO
40
41 and LUMO. For bias voltages larger than +2.5 V the reduction in the apparent corrugation of the
42
43 moiré pattern and its subsequent inversion³⁹ hinders the precise identification of the adsorption
44
45 site of the molecular attachments.
46
47
48
49
50
51
52
53
54
55
56
57
58
59
60



1
2
3 **Figure 2.** (a)-(f) $10 \times 10 \text{ nm}^2$ STM images with different bias voltages acquired at 80 K after
4 exposing gr/Ru(0001) to 180 Langmuir of acetonitrile at 300 K. Notice the related presence of
5 seven bright bumps on HCP-Top sites (marked with a white circle), one on FCC-Top site and
6 one graphene point defect (marked with a black circle). (g) Differential conductance, dI/dV ,
7 curves recorded at 80 K with the tip of the STM placed on top of the molecular attachments
8 (green), the FCC-Top, HCP-Top (purple and blue, respectively) and the ripples (black) areas of
9 the moiré pattern of gr/Ru(0001). The dI/dV individual curves were measured in open feedback
10 loop conditions with the tunneling gap stabilized at +0.3V and 50pA. The lock-in signal was
11 acquired using a modulation in the bias voltage of 40mV (rms), a frequency of 856 Hz and a
12 time constant of 10 ms.
13
14
15
16
17
18
19
20
21
22
23
24
25
26

27
28 Remarkably, single molecular attachments can be observed exclusively at the valleys of the
29 moiré pattern. Moreover, there is a strong preference for HCP-Top sites over FCC-top regions
30 offering another level of selectivity. For higher coverages on the order of 0.50 acetonitrile
31 molecules per moiré unit cell, $98.0 \pm 1\%$ of the HCP-Top and $2 \pm 1\%$ of the FCC-Top areas of the
32 unit cells are occupied. The same site preference has been observed for TCNQ⁴⁰ and F4-TCNQ⁴¹
33 molecules adsorbed on gr/Ru(0001) and can be understood considering the difference in the
34 electronic structure between the FCC-Top and HCP-Top areas.⁴⁰
35
36
37
38
39
40
41
42
43
44

45 In the present case, however, the bonding between the adsorbed molecular attachments and
46 graphene relies on a strong C-C covalent bond, which modifies the sp^2 hybridization of a single
47 C atom in graphene. This is demonstrated in Figure 3, in which a region containing three
48 molecular attachments located in HCP-Top regions, encircled in white, is imaged with atomic
49 resolution. The STM image has been taken in conditions where the molecular attachment is
50 transparent (2 mV bias and 800 pA current) because the small bias voltage is probing the energy
51
52
53
54
55
56
57
58
59
60

1
2
3 gap between HOMO and LUMO of the adsorbed molecule. Accordingly, the tip does not move
4
5 up when is located on top of the molecules attached to the surface. Simultaneously, the C atoms
6
7 with a modified hybridization where the three molecules are bonded appear as single atom
8
9 “holes” (see Supporting Information F.3 and Fig. S7 for details). Remarkably, the covalent
10
11 attachments are located exclusively on crystallographically identical carbon atoms of the
12
13 graphene overlayer. The inset shows the bright bumps of the molecules adsorbed in the “hole”
14
15 sites by restoring a bias voltage where they can be imaged through their LUMO orbitals. In spite
16
17 of the harsh imaging conditions all three molecules remain in place without any noticeable
18
19 change in shape or position. Going down to atomic resolution parameters without sweeping the
20
21 molecular attachments away during the scan is contrary to what happens with physisorbed or
22
23 even strongly chemisorbed isolated molecules, such as TCNQ⁹ or F₄-TCNQ⁴², indicating the
24
25 covalent nature of their attachment to graphene. In fact, the molecular attachments cannot be
26
27 displaced from their adsorption sites by the STM tip following standard manipulation
28
29 techniques.^{43,44} Annealing the sample in UHV further confirms the strong bond between
30
31 graphene and the molecular attachments. The sample remains unaltered up to 573K.
32
33
34
35
36
37
38
39
40
41
42
43
44
45
46
47
48
49
50
51
52
53
54
55
56
57
58
59
60

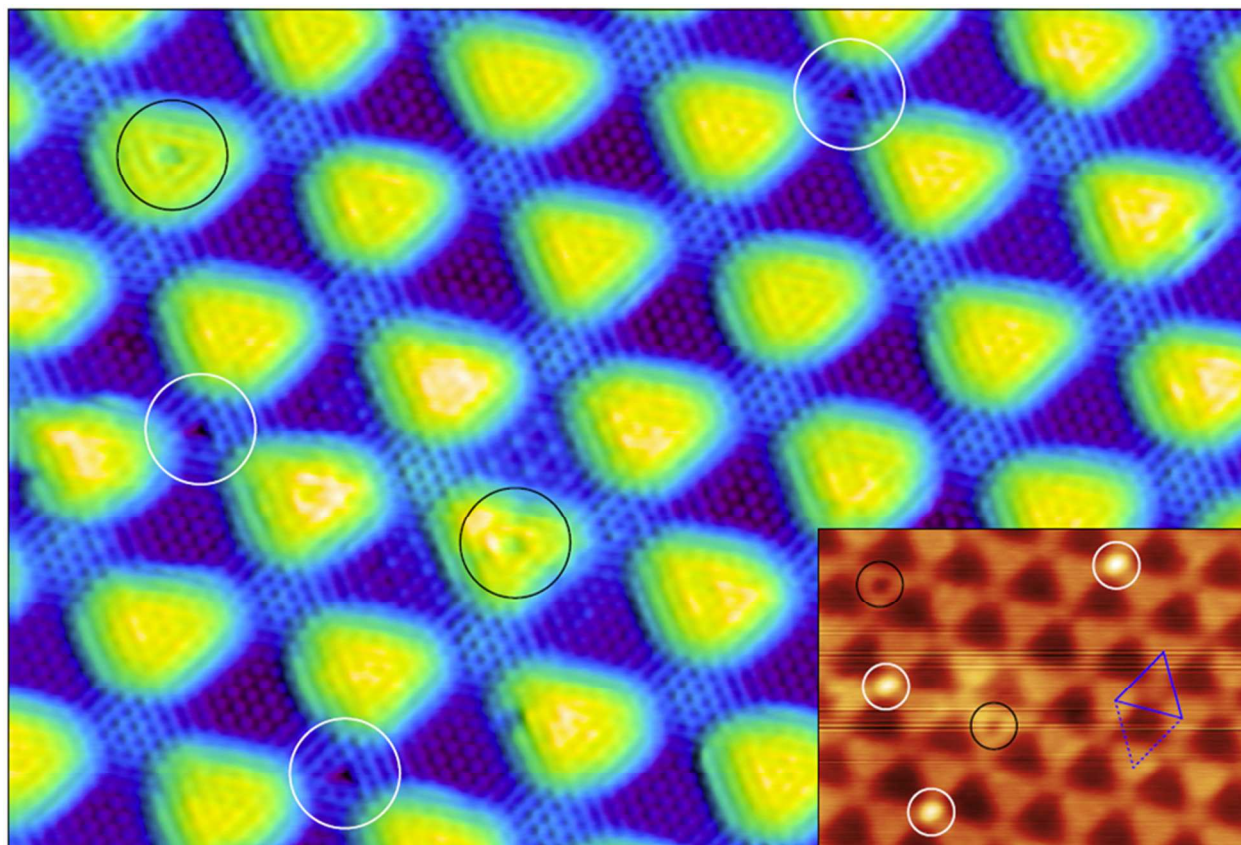


Figure 3. High resolution STM image ($17 \times 12 \text{ nm}^2$, $V_b = 2 \text{ mV}$, $I_t = 800 \text{ pA}$), acquired at 80 K on a region containing three molecular species (white circles) and two oxygen-related defects on graphene (black circles). Inset: Same region scanned afterwards with $V_b = +1.7 \text{ V}$ and $I_t = 100 \text{ pA}$. All three molecular attachments are still in place. The moiré unit cell is highlighted in blue in the inset.

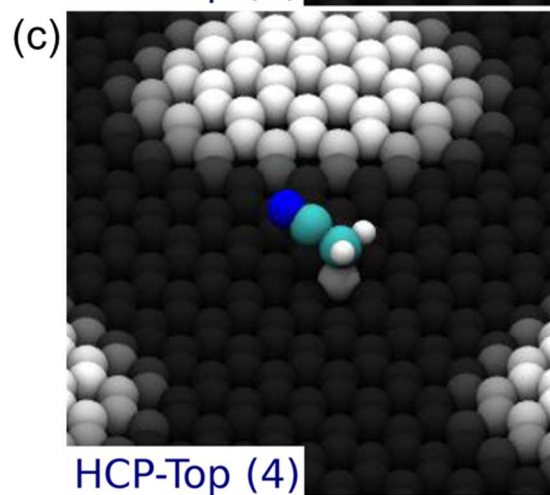
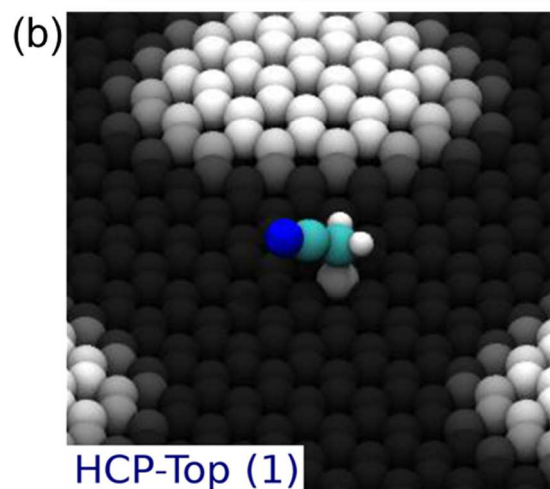
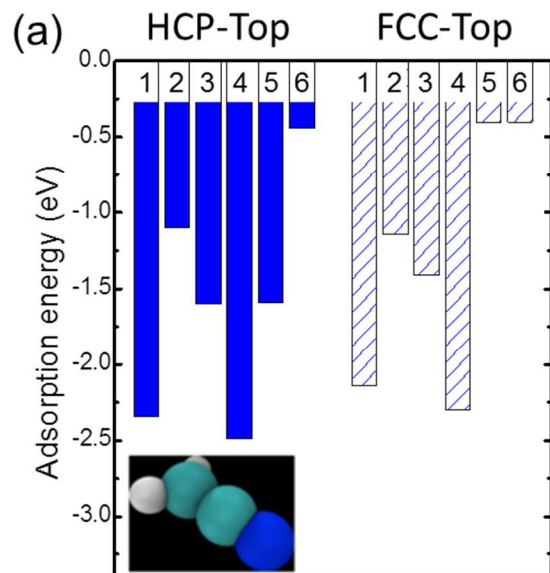
These facts confirm the selective covalent patterning of gr/Ru(0001) through treatment with CH_3CN beyond reasonable doubt. Given the relatively inert nature of CH_3CN , and knowing that under high-vacuum (10^{-6} Torr) conditions ion gauges produce and emit active chemical species through ionization of the residual gases in the vacuum chamber, which can be adsorbed onto graphene,⁴⁵ we reasoned the same process may take place during the exposure of the graphene surface to the acetonitrile molecules in UHV, since we use an ion gauge to measure the partial

1
2
3 pressure of the acetonitrile gas. In order to gather experimental evidence of the molecular
4
5 fragments that can be produced in the ion gauge during the CH₃CN exposition, we introduced in
6
7 the UHV chamber the same partial pressure (1×10^{-6} Torr) of acetonitrile used during the
8
9 graphene exposure and recorded the mass spectrum of the gas utilizing a quadrupole mass
10
11 spectrometer (QMS) (see Supporting Information D for details). The ionization chamber of the
12
13 QMS works under the same physical principle as the ion gauges and therefore the spectra
14
15 measured is a reliable indicator of the chemical species produced in the ion gauge. The m/z
16
17 pattern is perfectly consistent with a significant concentration of CH₂CN[•] (Figure S3 and
18
19 Supporting Information D for details). It is well known that CH₂CN[•] can be generated directly
20
21 from CH₃CN by homolytic cleavage of a C-H bond.⁴⁶⁻⁴⁸ Moreover, the cyanomethyl radical
22
23 (CH₂CN[•]) is known to react with C-C double bonds⁴⁹⁻⁵¹ and arenes⁵² forming C-C bonds.
24
25
26
27
28
29

30 To provide further experimental evidence for this hypothesis we exposed the sample to 180
31
32 Langmuir of acetonitrile with the ion gauge in the preparation chamber turned *off* and under
33
34 these conditions *no* molecular attachments were detected on the surface (see Supporting
35
36 Information G for further details).
37
38
39

40 To gain atomic understanding of the reaction, we ran DFT calculations for the adsorption of
41
42 CH₂CN[•] on gr/Ru(0001). The results are summarized in Figure 4. In agreement with the
43
44 experimental data, the adsorption energies are within the limits of a covalent bond (>2.1 eV)(see
45
46 Figure 4(a)). Remarkably, the HCP-Top/FCC-Top preference we observe experimentally is also
47
48 reproduced. The two most stable configurations, HCP-Top(1) and HCP-Top(4), with adsorption
49
50 energies of 2.34 eV and 2.49 eV are shown in Fig. 4(c), and Fig. 4(d). In this case, it is the alkyl
51
52 carbon atom of CH₂CN[•] that lies closer to the graphene surface, as is observed in the
53
54 cyanomethylation of arenes.⁵² The graphene carbon atom immediately below the CH₂CN
55
56
57
58
59
60

1
2
3 addend is clearly displaced from the graphene mesh (see Supporting Information F for details).
4
5
6 The shortest distance between an acetonitrile carbon atom and a graphene atom are 1.60 Å and
7
8 1.58 Å for the acetonitrile in the HCP-Top (1) and HCP-Top(4) adsorption geometries shown in
9
10 Fig. 4(c) and Fig. 4(d), in very good accordance with a C-C single bond, for which the textbook
11
12 C-C distance is 1.54 Å.⁵³ Other configurations considered and the corresponding adsorption
13
14 energies are shown in Table S1 and Figure S6 and discussion in section F.3 of the SI. In contrast,
15
16 identical calculations run with CH₃CN resulted in adsorption energies of 0.40 ± 0.03 eV and
17
18 0.42 ± 0.02 eV for the HCP-top and FCC-top regions, respectively, with the shortest acetonitrile-
19
20 graphene distances > 3 Å, indicative of physisorption, as expected (see table S2 and Figure S8 in
21
22 section F.3 of the SI).
23
24
25
26
27
28
29
30
31
32
33
34
35
36
37
38
39
40
41
42
43
44
45
46
47
48
49
50
51
52
53
54
55
56
57
58
59
60



1
2
3 **Figure 4.** (a) Adsorption energies calculated for the different configurations of CH₂CN* on the
4 HCP-top (solid boxes) and on the FCC-Top (empty boxes) regions of the gr/Ru(0001) moiré.
5
6 The inset shows the ground state geometry of the corresponding molecule in the gas-phase. (b)
7
8 and (c), Ground state adsorption geometries of the two most stable configurations of CH₂CN*
9
10 adsorbed in the HCP-Top region of the gr/Ru(0001) moiré. Graphene atoms are colored from
11
12 dark-gray to white depending on their height. Carbon, nitrogen and hydrogen atoms of the
13
14 molecule are colored in cyan, blue and white.
15
16
17
18
19

20
21 To investigate the role of the Ru metallic substrate we synthesised graphene on Ir(111)
22
23 (hereafter, gr/Ir(111)), a system which exhibits a similar moiré pattern⁵⁴ but with almost
24
25 negligible charge transfer and interaction between the carbon and iridium. Exposing gr/Ir(111)
26
27 to 1×10⁻⁶ Torr of CH₃CN, no CH₂CN* attachments were observed, confirming that the strong
28
29 interaction between Ru and the graphene overlayer plays a fundamental role in the covalent
30
31 functionalization (see Supporting Information E for details).
32
33
34
35

36 Due to the strong interaction between graphene and the Ru(0001) surface, the moiré pattern not
37
38 only presents specific atomic sites with high chemical reactivity but long range order as well. In
39
40 this system it is possible to grow graphene layers presenting lateral domain sizes exceeding 300
41
42 nm.^{39,55} The large domain size together with the exquisite spatial selectivity of our
43
44 functionalization method ensures the long range order of the functionalized surface. Figure 5
45
46 shows a 66 x 40 nm² STM image of the functionalized gr/Ru(0001). In the image 50% of the
47
48 moiré unit cells are occupied by one chemically bonded – CH₂CN molecule. Of those 98.6% are
49
50 bonded in the HCP-Top areas, while only 1.4% of the – CH₂CN are bonded to the FCC-TOP
51
52 areas.
53
54
55
56
57
58
59
60

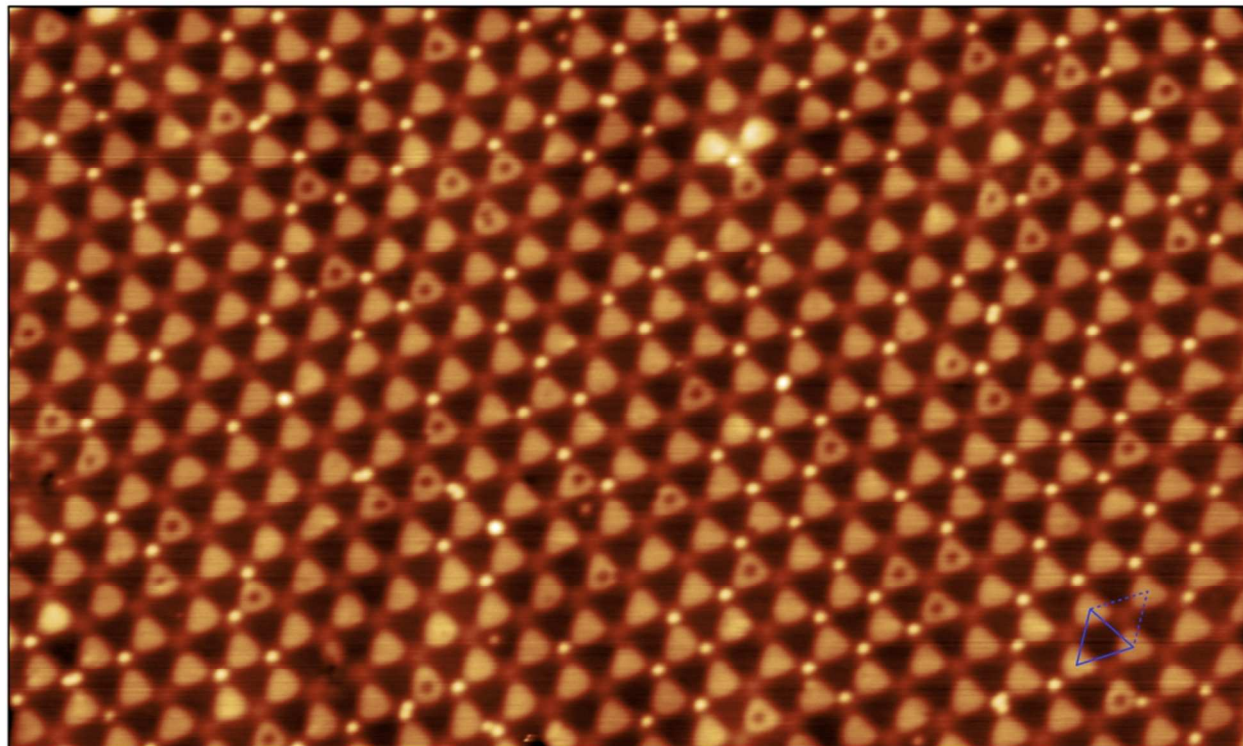


Figure 5. STM image ($66 \times 40 \text{ nm}^2$, $V_b = 1.7 \text{ V}$, $I_t = 30 \text{ pA}$) acquired at 80 K on a high coverage sample, prepared by exposing the gr/Ru(0001) surface to 600 Langmuir of acetonitrile at 300 K. The moiré unit cell is highlighted in blue.

Similar results have been obtained for propionitrile, isobutyronitrile and 2-phenylacetonitrile, demonstrating the applicability of this functionalization method to other molecular species (see Supporting Information H for details).

In conclusion, we take advantage of the nanostructuration induced on graphene grown on Ru(0001) to chemically functionalize the graphene overlayer with atomic-level selectivity and exquisite spatial periodicity. The comparison between graphene grown on Ir(111) and graphene on Ru(0001) shows the importance of the interaction between the graphene and the metallic substrate that spatially modulates the properties of the graphene. Acetonitrile is homolytically

1
2
3 broken by electron bombardment producing cyanomethyl radicals that react with the
4
5 nanostructured graphene in a spatially modulated fashion. These results offer the possibility for
6
7 tuning the graphene electronic, optic or magnetic properties through an adequate covalent
8
9 functionalization of single layer graphene with long-range order on the order of hundreds of
10
11 nanometers and a periodicity of almost 3 nm. Moreover, identical results were obtained for
12
13 propionitrile, isobutyronitrile and 2-phenylacetonitrile, establishing a benchmark for the
14
15 attachment of more complex molecular structures to specific atomic sites on graphene.
16
17
18
19

20 21 **Methods.**

22
23
24 All experiments were performed in an UHV chamber with a base pressure of 5×10^{-11} Torr
25
26 equipped with a low-temperature STM and facilities for tip and sample preparation. All the STM
27
28 measurements were carried out at 80 K. The graphene layer was prepared by keeping the Ru
29
30 crystal at 1150 K in UHV while exposing it to an ethylene partial pressure of 8×10^{-8} Torr for 10
31
32 min. Acetonitrile was introduced in the UHV chamber via a leak valve to produce a partial
33
34 pressure of 1×10^{-6} Torr. The values for the partial pressures of the different gases are measured
35
36 using a Bayard-Alpert gauge calibrated for N_2 . The details of the calculations are provided in the
37
38 Supporting Information.
39
40
41
42

43 44 ASSOCIATED CONTENT

45
46
47 **Supporting Information.** Detailed discussion of the graphene/Ru(0001) structure. Oxygen
48
49 contamination identification. Wet chemistry approach. Relative abundance of the cyanomethyl
50
51 radical versus the acetonitrile molecule. Adsorption on graphene/ Ir(111). Theoretical
52
53 calculations. Ion gauge influence on the functionalization. Functionalization with different
54
55
56
57
58
59
60

1
2
3 molecules ($\text{CH}_3\text{CH}_2\text{CN}$, $(\text{CH}_3)_2\text{CHCN}$ and $\text{Ph-CH}_2\text{CN}$). This material is available free of charge
4
5 via the Internet at <http://pubs.acs.org>.”
6
7

8 9 AUTHOR INFORMATION

10 11 **Corresponding Author**

12
13 * (A.L.V.d.P.) al.vazquezdeparaga@uam.es; (E.M.P.) emilio.perez@imdea.org
14
15
16

17 18 **Present Addresses**

19
20 † Center for nanostructured Graphene, Department of Micro- and Nanotechnology, Technical
21
22 University of Denmark, Ørstedes plads, Building 345B, DK-2800 Kgs., Lyngby, Denmark.
23
24

25
26 ‡ Physik-Department E20, TU München, James-Franck str. 1, D-85748 Garching, Germany
27
28

29 30 **Author Contributions**

31
32 The experiments and data analysis were carried out primarily by F.C., J.J.N, with important
33
34 contributions by A.B., R.B.-G. and M.G. S.L. performed the wet chemistry experiments. D.S.
35
36 performed the theoretical calculations and contributed to the writing of the manuscript. D.G.
37
38 contributed with the data analysis and contributed to the writing to the manuscript. R.M.
39
40 contributed to the writing of the manuscript. E.M.P. and A.L.V.P. designed the experiments and
41
42 wrote the manuscript with contributions from all authors.
43
44
45
46

47 48 **Notes**

49
50 The results described here are partially protected under Spanish patent application P201530126.
51
52

53 54 **ACKNOWLEDGMENT**

55
56
57
58
59
60

1
2
3 Financial support by the European Research Council (MINT, ERC-StG- 2012-307609) the
4
5 Ministerio de Economía y Competitividad (MINECO) FIS2013-40667-P and CTQ2014-60541-
6
7 P, and Comunidad de Madrid through the programme MAD2D P2013/MIT-3007 and
8
9 Nanofrontmag S2013/MIT-2850 is gratefully acknowledged. D.G. acknowledges RyC-2012-
10
11 09864. R.B.-G. acknowledges BES-2011-050821.
12
13
14

15 REFERENCES

- 16
17 1. Geim, A. K.; Novoselov, K. S. *Nature Mater.* **2007**, *6*, 183-191.
- 18
19
20
21 2. Georgakilas, V.; Otyepka, M.; Bourlinos, A.B.; Chandra, V.; Kim, N.; Kemp, K.C.; Hobza, P.;
22
23 Zboril, R.; Kim, K.S. *Chem. Rev.* **2012**, *112*, 6156-6214.
- 24
25
26
27 3. Chua, C. K.; Pumera, M. *Chem. Soc. Rev.* **2013**, *42*, 3222-3233.
- 28
29
30
31 4. Park, J.; Yan, M. *Acc. Chem. Res.* **2013**, *46*, 181-189.
- 32
33
34
35 5. Kuila, T.; Bose, S.; Kumar, A.; Khanra, P.; Kim, N.H.; Lee, J.H. . *Progress in Materials*
36
37 *Science* **2012**, *57*, 1061-1105.
- 38
39
40
41 6. Sun, Z.; James; D.K; Tour, J.M. *J. Phys. Chem. Lett.* **2011**, *2*, 2425-2432.
- 42
43
44
45 7. Criado, A.; Melchiona, M.; Marchesan, S.; Prato, M. *Angew. Chem. Int. Ed.* **2015**, *54*, 10734-
46
47 10750.
- 48
49
50
51 8. Criado, A.; Melchiona, M.; Marchesan, S.; Prato, M. *Angew. Chem. Int. Ed.* **2015**, *54*, 2-19.
- 52
53
54
55 9. Schedin, F.; Geim, A.K.; Morozov, S.V.; Hill, E.W.; Blake, P.; Katsnelson, M.I.; Novoselov,
56
57 K.S. *Nature Mater.* **2007**, *6*, 652-655.
58
59
60

- 1
2
3
4
5
6
7
8
9
10
11
12
13
14
15
16
17
18
19
20
21
22
23
24
25
26
27
28
29
30
31
32
33
34
35
36
37
38
39
40
41
42
43
44
45
46
47
48
49
50
51
52
53
54
55
56
57
58
59
60
10. Garnica, M.; Stradi, D.; Barja, S.; Calleja, F.; Díaz, C.; Alcamí, M.; Vázquez de Parga, A.L.; Martín, F.; Miranda, R. *Nature Phys.* **2013**, *9*, 368-374.
11. Vinogradov, N.A.; Schulte, K.; Ng, M.L.; Mikkelsen, A.; Lundgren, E.; Mårtensson, N.; Preobrajenski, A.B. *J. Phys. Chem. C* **2011**, *115*, 9568-9577.
12. Hossain, M.Z.; Johns, J.E.; Bevan, K.H.; Kamel, H.J.; Liang, Y.T.; Yoshimoto, S.; Mukai, K.; Koitaya, T.; Yoshinobu, J.; Kawai, M.; Lear, A.M.; Kesmodel, L.L.; Tait, S.L.; Hersam, M.C. *Nature Chem.* **2012**, *4*, 305-309.
13. Sofo, J.O.; Chaudhari, A.S.; Barber, G.D. *Phys. Rev. B* **2007**, *75*, 153401.
14. Boukhvalov, D.W.; Katsnelson, M.I.; Lichtenstein, A.I. *Phys. Rev. B* **2008**, *77*, 035427.
15. Elias, D. C.; Nair, R.R.; Mohiuddin, T.M.G.; Morozov, S.V.; Blake, P.; Halsall, M.P.; Ferrari, A.C.; Boukhvalov, D.W.; Katsnelson, M.I.; Geim, A.K.; Novoselov, K.S. *Science* **2008**, *323*, 610-613.
16. Haberer, D.; Vyalikh, D.V.; Taioli, S.; Dora, B.; Farjam, M.; Fink, J.; Marchenko, D.; Pichler, T.; Ziegler, K.; Simonucci, S.; Dresselhaus, M.S.; Knupfer, M.; Büchner, B.; Grüneis, A. *Nano Lett.* **2010**, *10*, 3360-3366.
17. Park, C.H.; Yang, L.; Son, Y.W.; Cohen, M.L.; Louie, S.G. *Nature Phys.* **2008**, *4*, 213-217.
18. Ouyang, F.; Peng, S.; Liu, Z.; Liu, Z. *ACS Nano* **2011**, *5*, 4023-4030.
19. Dvorak, M.; Oswald, W.; Wu, Z. *Sci. Rep.* **2013**, *3*, 2289.

- 1
2
3
4
5
6
7
8
9
10
11
12
13
14
15
16
17
18
19
20
21
22
23
24
25
26
27
28
29
30
31
32
33
34
35
36
37
38
39
40
41
42
43
44
45
46
47
48
49
50
51
52
53
54
55
56
57
58
59
60
20. Bian, S.; Scott, A.M.; Cao, Y.; Liang, Y.; Osuna, S.; Houk, K.N.; Braunschweig, A.B. *J. Am. Chem. Soc.* **2013**, *135*, 9240-9243.
21. Hossain, M.Z.; Walsh, M.A.; Hersam, M.C. *J. Am. Chem. Soc.* **2010**, *132*, 15399-15403.
22. Wu, Q.; Wu, Y.; Hao, Y.; Geng, J.; Charlton, M.; Chen, S.; Ren, Y.; Ji, H.; Li, H.; Boukhvalov, D.W.; Piner, R.D.; Bielawski, C.W.; Ruoff, R.S. *Chem. Commun.* **2013**, *49*, 677-679.
23. Bissett, M. A.; Konabe, S.; Okada, S.; Tsuji, M.; Ago, H. *ACS Nano* **2013**, *7*, 10335-10343.
24. Vázquez de Parga, A.L.; Miranda, R. In *Graphene: Properties, preparation, characterisation and devices*; Chap 6; Skakalova, V., Kaiser, A.B., Eds.; Woodhead Publishing, (2014).
25. Balog, R.; Jørgensen, B.; Nilsson, L.; Andersen, M.; Rienks, E.; Bianchi, M.; Fanetti, M.; Laegsgaard, E.; Baraldi, A.; Lizzit, S.; Slijvancanin, Z.; Besenbacher, F.; Hammer, B.; Pedersen, T.G.; Hofmann, P.; Hornekaer, L. *Nature Mater.* **2010**, *9*, 315-319.
26. Balog, R.; Andersen, M.; Jørgensen, B.; Slijvancanin, Z.; Hammer, B.; Baraldi, A.; Larciprete, R.; Hofmann, P.; Hornekaer, L.; Lizzit, S., *ACS Nano* **2013**, *7*, 3823-3832.
27. Coraux, J; N'Diaye, A.T.N.; Buss, C.; Michely, T. *Nano Lett.* **2008**, *8*, 565-570.
28. Loginova, E.; Nie, S.; Thumer, K.; Bartelt, N.C.; McCarty, K.F. *Phys. Rev. B* **2009**, *80*, 085430.
29. Chae, S. J.Günes, F.; Kim, K.K.; Kim, E.S.; Han, G.H.; Kim, S.M.; Shin, H.J.; Yoon, S.M., Choi, J.Y.; Park, M.H.; Yang, C.W.; Pribat, D.; Lee, Y.H. *Adv. Mater.* **2009**, *21*, 2328-2333.

- 1
2
3 30. Reina, A.; Jia, X.; Ho, J.; Nezich, D.; Son, H.; Bulovic, V.; Dresselhaus, M.S.; Kong, J. *Nano*
4
5 *Lett.* **2009**, *9*, 30-35.
6
7
8
9 31. Li, X.; Cai, X.; An, J.; Kim, S.; Nah, J.; Yang, D.; Piner, R.; Velamakanni, A.; Jung, I.;
10
11 Tutuc, E.; Banerjee, S.K.; Colombo, L.; Ruoff, R.S. *Science* **2009**, *324*, 1312-1314.
12
13
14
15 32. Lee, Y.; Bae, S.; Jang, H.; Jang, S.; Zhu, S.E.; Sim, S.H.; Song, Y.I.; Hong, B.H.; Ahn, J.H.
16
17 *Nano Lett.* **2010**, *10*, 490-493.
18
19
20
21 33. Preobrajenski, A.B.; Ng, M.L.; Vinogradov, A.S.; Martensson, N. *Phys. Rev. B* **2008**, *78*,
22
23 073401.
24
25
26
27 34. Vazquez de Parga, A. L.; Calleja, F.; Borca, B.; Hinarejos, J.J.; Passeggi, M.G.C.; Guinea,
28
29 F.; Miranda, R.. *Phys. Rev. Lett.* **2008**, *100*, 056807.
30
31
32
33 35. Stradi, D.; Barja, S.; Díaz, C.; Garnica, M.; Borca, B.; Hinarejos, J.J.; Sánchez-Portal, D.;
34
35 Alcamí, M.; Arnau, A.; Vázquez de Parga, A.L.; Miranda, R.; Martín, F. *Phys. Rev. B* **2013**, *88*,
36
37 245401.
38
39
40
41 36. Stradi, D.; Barja, S.; Díaz, C.; Garnica, M.; Borca, B.; Hinarejos, J.J.; Sánchez-Portal, D.;
42
43 Alcamí, M.; Arnau, A.; Vázquez de Parga, A.L.; Miranda, R.; Martín, F. *Phys. Rev. Lett.* **2011**,
44
45 *106*, 186102.
46
47
48
49 37. Borca, B.; Barja, S.; Garnica, M.; Sánchez-Portal, D.; Silkin, V.M.; Chulkov, E.V.;
50
51 Hermanns, C.F.; Hinarejos, J.J.; Vázquez de Parga, A.L.; Arnau, A.; Echenique, P.M.; Miranda,
52
53 R. *Phys. Rev. Lett.* **2010**, *105*, 036804.
54
55
56
57 38. Katano, S.; Kim, Y.; Trenary, M.; Kawai, M. *Chem. Commun.* **2013**, *49*, 4679-4681.
58
59
60

- 1
2
3
4 39. Borca, B.; Barja, S.; Garnica, M.; Minniti, M.; Politano, A.; Rodríguez-García, J.M.;
5
6 Hinarejos, J.J., Farías, D.; Vázquez de Parga, A.L.; Miranda, R. *New J. Phys.* **2010**, *12*, 093018.
7
8
9 40. Garnica, M.; Stradi, D.; Calleja, F.; Barja, S.; Díaz, C.; Alcamí, M.; Arnau, A.; Vázquez de
10
11 Parga, A.L.; Martín, F.; Miranda, R. *Nano Lett.* **2014**, *4*, 4560-4567.
12
13
14 41. Stradi, D.; Garnica, M.; Díaz, C.; Calleja, F.; Barja, S.; Alcamí, M.; Martín, N.; Arnau, A.;
15
16 Vázquez de Parga, A.L.; Miranda, R.; Martín, F. *Nanoscale* **2014**, *6*, 15271-15279.
17
18
19 42. Barja, S., Garnica, M.; Hinarejos, J.J.; Vázquez de Parga, A.L.; Martín, N.; Miranda, R.,
20
21
22 *Chem. Comm.* **2010**, *46*, 8198-8200.
23
24
25 43. Stroschio, J. A.; Eigler, D. M. *Science* **1991**, *254*, 1319-1326.
26
27
28 44. Hla, S.-W. *J. Vac. Sci. Technol., B* **2005**, *23*, 1351-1360.
29
30
31 45. Caillier, C.; Ki, D.K.; Lisunova, Y.; Gaponenko, I.; Paruch, P.; Morpugo, A.F.
32
33
34 *Nanotechnology* **2013**, *24*, 405201.
35
36
37 46. Lalevee, J.; Allonas, X.; Fouassier, J.-P. *J. Org. Chem.* **2005**, *70*, 814-819.
38
39
40 47. Henry, D.J.; Parkinson, C.J.; Mayer, P.M.; Radom, L. *J. Phys. Chem. A* **2001**, *105*, 6750-
41
42
43 6756.
44
45
46 48. Coote, M.L. *J. Phys. Chem. A* **2004**, *108*, 3865-3872.
47
48
49 49. Kukk, E.; Sankari, R.; Huttula, M.; Sankari, A.; Aksela, H.; Aksela, S. *J. Electron Spectrosc.*
50
51
52 *Relat. Phenom.* **2007**, *155*, 141-147.
53
54
55 50. Wu, J. Q.; Beranek, I.; Fischer, H. *Helv. Chim. Acta* **1995**, *78*, 194-214.
56
57
58
59
60

1
2
3 51. Wong, M. W.; Radom, L. *J. Phys. Chem.* **1995**, *99*, 8582-8588.
4

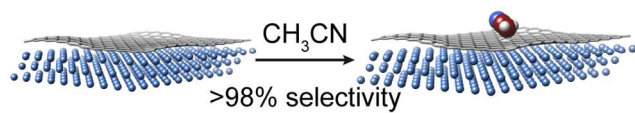
5
6 52. Yoshida, H.; Fujimura, Y.; Yuzawa, H.; Kumagai, J.; Yoshida, T. *Chem. Commun.* **2013**, *49*,
7
8 3793-3795.
9

10
11 53. Cottrell, T. L. *The Strengths of Chemical Bonds*. Butterworth Scientific (1978)
12

13
14 54. N'Diaye, A.T.; Coraux, J.; Plasa, T.N.; Busse, C.; Michely, T. *New J. Phys.* **2008**, *10*,
15
16 043033.
17
18

19
20 55. Sutter, P.W.; Flege, J.I.; Sutter, E.A. *Nature Mater.* **2008**, *7*, 406-500.
21
22
23
24
25
26
27
28
29
30
31
32
33
34
35
36
37
38
39
40
41
42
43
44
45
46
47
48
49
50
51
52
53
54
55
56
57
58
59
60

TOC graphics



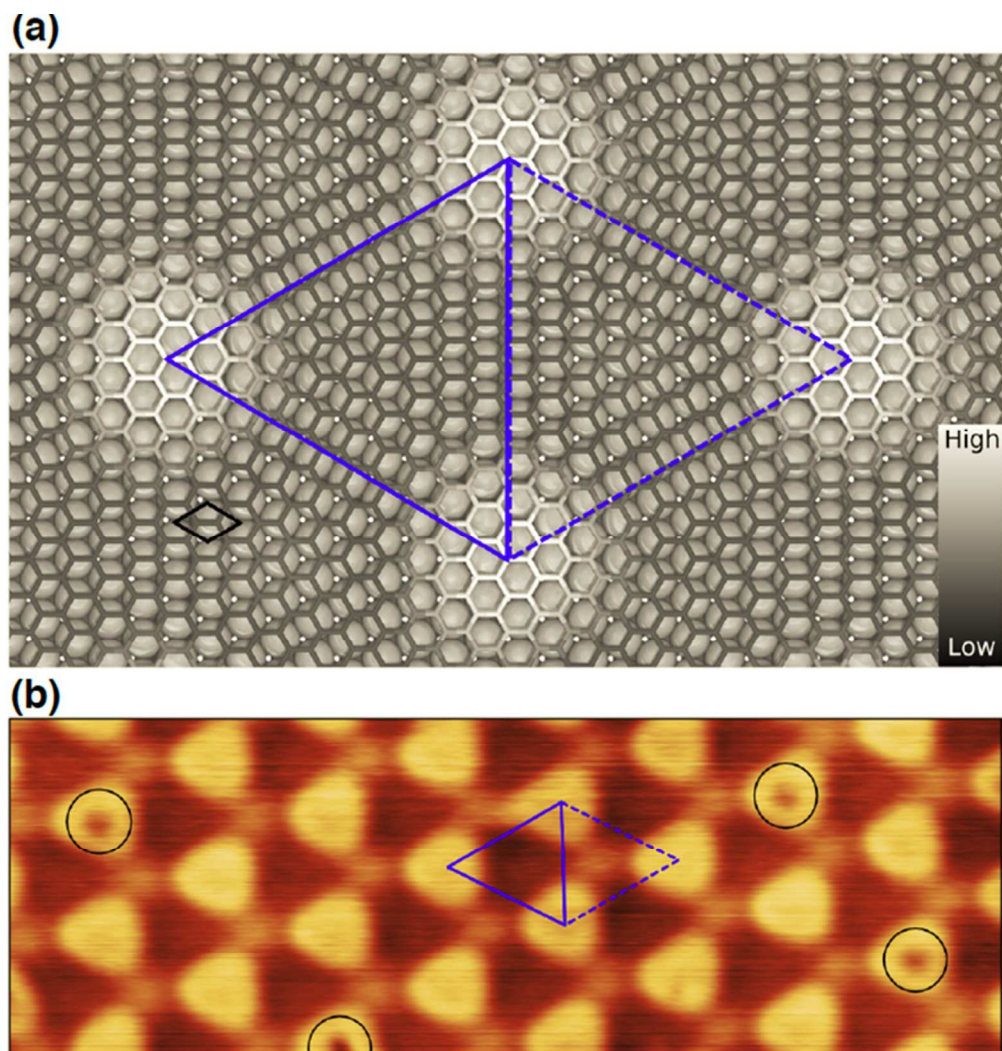


Figure 1. (a) Ball model of the gr/Ru(0001) surface, where grey circles represent the Ru atoms of the first atomic layer. The graphene hexagonal lattice is shown in a black to white color scale to indicate the height of the carbon atoms respect to the Ru(0001) surface. The unit cell of the moiré pattern is highlighted by two blue triangles. At the vertices all carbon atoms fall on threefold hollow sites of the Ru(0001) surface. At the center of the solid (dashed) triangle one carbon sub-lattice falls on FCC-stacked (HCP-stacked) threefold hollow sites and the other one on top positions. These two regions are named "FCC-Top" and "HCP-Top" respectively. (b) STM image acquired on pristine gr/Ru(0001) ($24 \times 7 \text{ nm}^2$; $V_b = +1.5 \text{ V}$, $I_t = 30 \text{ pA}$). The moiré pattern arising from the lattice mismatch is highlighted in blue. The HCP-Top area is marked with the dashed triangle and the FCC-Top area is marked the solid triangle. Four point defects on the atop areas are indicated by black circles.

189x195mm (103 x 104 DPI)

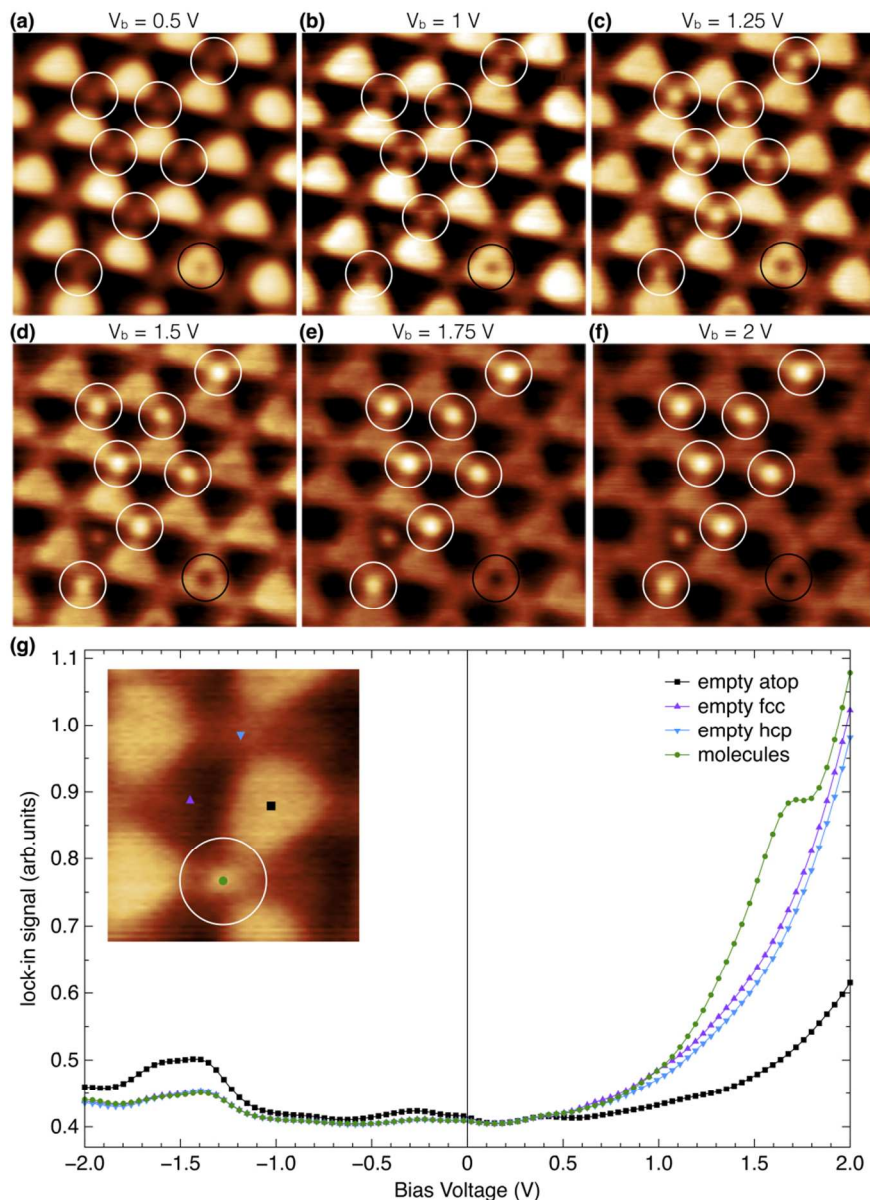


Figure 2. (a)-(f) $10 \times 10 \text{ nm}^2$ STM images with different bias voltages acquired at 80 K after exposing gr/Ru(0001) to 180 Langmuir of acetonitrile at 300 K. Notice the related presence of seven bright bumps on HCP-Top sites (marked with a white circle), one on FCC-Top site and one graphene point defect (marked with a black circle). (g) Differential conductance, dI/dV , curves recorded at 80 K with the tip of the STM placed on top of the molecular attachments (green), the FCC-Top, HCP-Top (purple and blue, respectively) and the ripples (black) areas of the moiré pattern of gr/Ru(0001). The dI/dV individual curves were measured in open feedback loop conditions with the tunneling gap stabilized at +0.3V and 50pA. The lock-in signal was acquired using a modulation in the bias voltage of 40mV (rms), a frequency of 856 Hz and a time constant of 10 ms.

152x208mm (171 x 171 DPI)

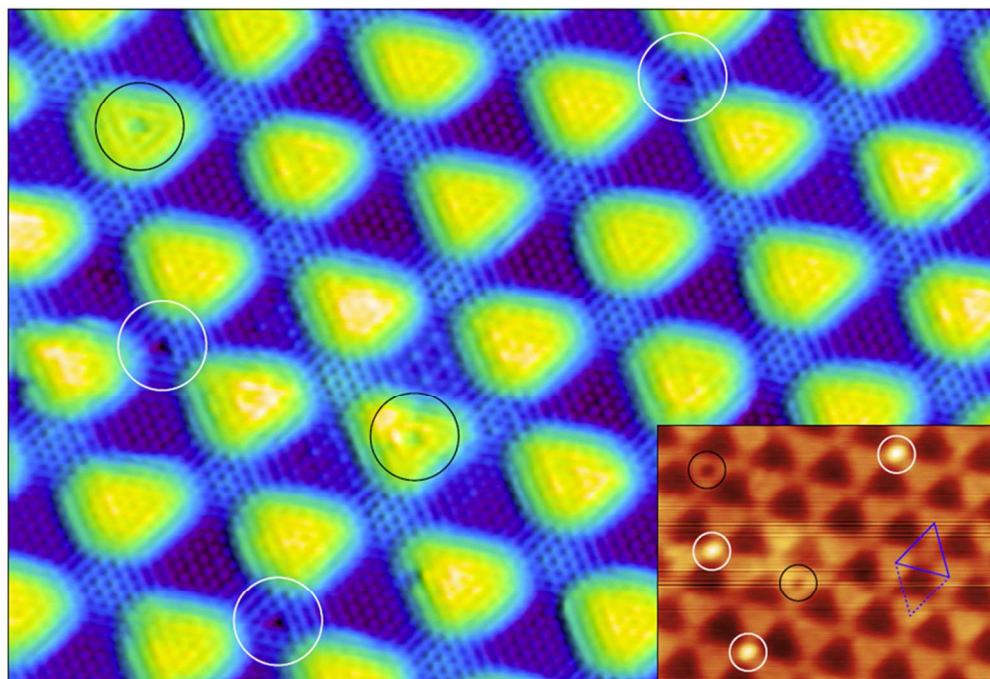
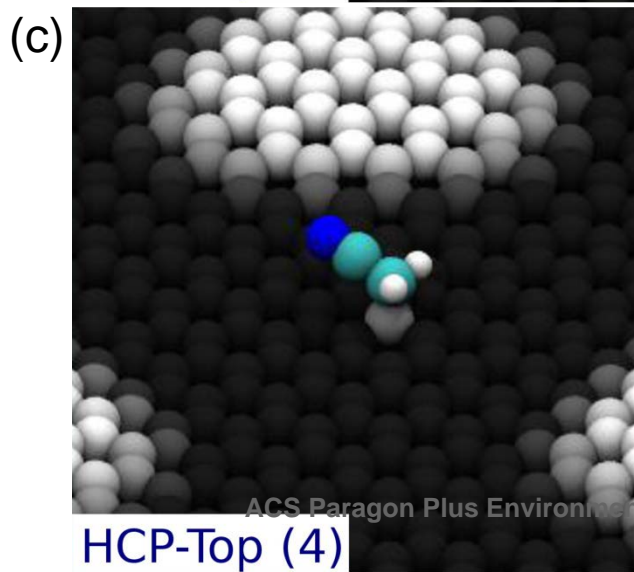
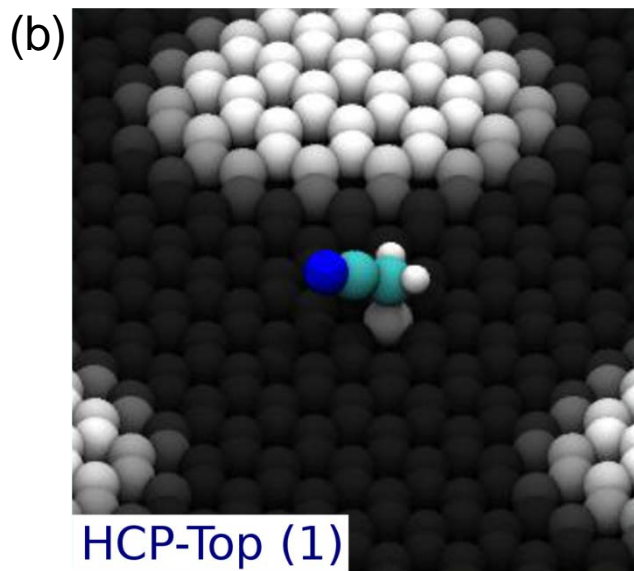
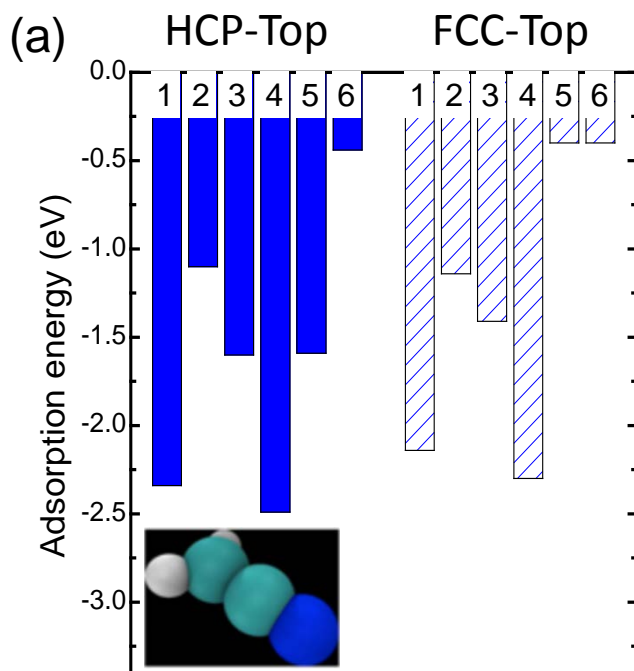


Figure 3. High resolution STM image ($17 \times 12 \text{ nm}^2$, $V_b = 2 \text{ mV}$, $I_t = 800 \text{ pA}$), acquired at 80 K on a region containing three molecular species (white circles) and two oxygen-related defects on graphene (black circles). Inset: Same region scanned afterwards with $V_b = +1.7 \text{ V}$ and $I_t = 100 \text{ pA}$. All three molecular attachments are still in place. The moiré unit cell is highlighted in blue in the inset.

180x122mm (138 x 138 DPI)



1
2
3
4
5
6
7
8
9
10
11
12
13
14
15
16
17
18
19
20
21
22
23
24
25
26
27
28
29
30
31
32
33
34
35
36
37
38
39
40
41
42
43
44
45
46
47
48
49
50
51
52
53
54
55
56
57
58

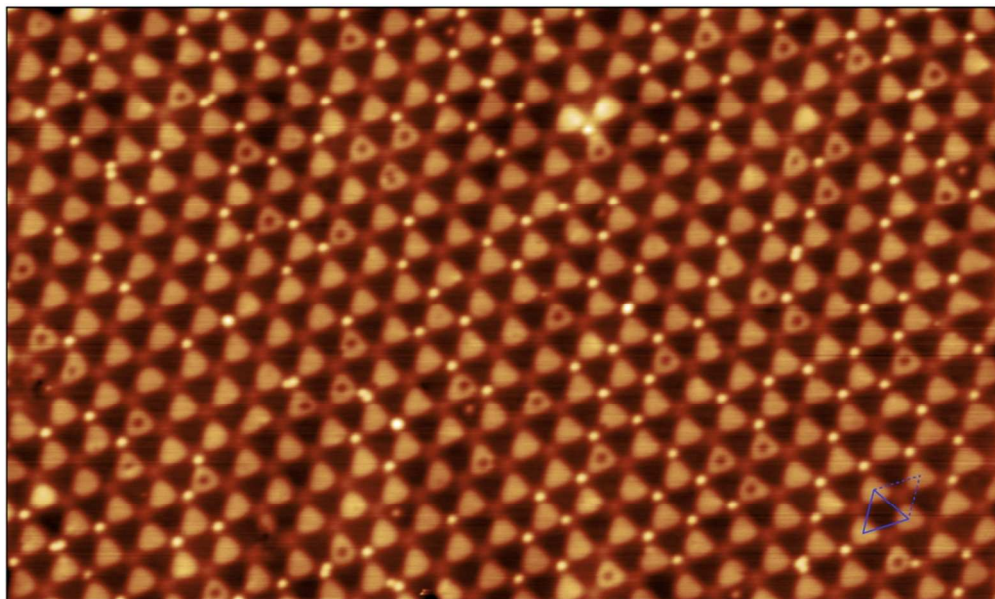


Figure 5. STM image ($66 \times 40 \text{ nm}^2$, $V_b = 1.7 \text{ V}$, $I_t = 30 \text{ pA}$) acquired at 80 K on a high coverage sample, prepared by exposing the gr/Ru(0001) surface to 600 Langmuir of acetonitrile at 300 K. The moiré unit cell is highlighted in blue.

180x108mm (144 x 144 DPI)